# Meteor radar interferometry using NEC antenna array simulations

Gabe A. Cohn and John D. Sahr

Department of Electrical Engineering, University of Washington, Seattle, Washington, USA

September 2006, revised March 2009

**Abstract.** Phase errors have a dramatic effect on the results of a meteor radar interferometer, and compensating for these errors is difficult. However, we present a new method of interferometry which accurately compensates for the mutual coupling between antennas placed very close to each other in an array. This new method of interferometery is based on computer modeling methods and the use of Numerical Electromagnetics Code (NEC), a method of moments EM simulator. The proposed method of interferometry not only locates the position of maximum likelihood for a meteor, but also plots the likelihood of the meteor's location across the whole sky.

## 1. Introduction

Meteor scatter events can be easily detected using current passive radar systems, such as the Manastash Ridge Radar (MRR) described in *Sahr and Lind* [1997]. In addition, methods described in *Meyer and Sahr* [2004] can be used to obtain range and Doppler data from the meteor scatter. However, accurately determining the direction of the meteor scatter is difficult. Common practice is to set up an array of antennas that can act as an interferometer. By measuring the phase differences between the antennas in an array, it is possible to determine the angle of arrival of the incoming radio wave [*Jones et al.*, 1998]. When complemented with range data, this can give the exact geophysical location of a meteor scatter event.

Unfortunately, there are several errors that can make these calculations inaccurate. Since interferometric data, such as angle of arrival, are calculated based on phase differences between antennas, any errors in phase will cause significant errors in all derived values. For this reason, *Holdsworth et al.* [2004] describes various methods for phase calibrations. These phase errors can be divided into two main categories: transmission errors and receiver equipment errors. Transmission errors are introduced when the radio wave travels through an imperfect medium from the transmitter to the receiver. Receiver equipment errors occur when the receiver equipment introduces phase shifts into the measured data. These phase shifts can come from many sources; however, only those phase shifts due to transmission line propagation and mutual coupling between antennas are considered in this paper. Other significant errors, including transmission errors are described in *Holdsworth et al.* [2004].

Phase shifts within the transmission lines that connect the antennas to the receiver can cause significant errors in the measured data at the receiver. If all of the transmission lines are not the same length, phase differences will be seen by the receiver even when all antennas are in phase. Luckily, these errors are linear, and therefore can be taken into consideration if the lengths of all transmission lines are accurately known.

In addition to phase shifts in the transmission lines, errors can occur due to the mutual coupling between the antennas in an array. This coupling is due to the mutual impedances between the antennas. Since the antennas are not isolated but in an array, it cannot be assumed that the voltages seen by the receivers represent those from isolated antennas. Since the effect of mutual coupling increases as the distance between the antennas decreases, significant errors can be introduced by closely spaced antennas. Unfortunately, this is a very difficult problem to take into account, and therefore most antenna arrays simply avoid the issue by making larger spacing between antennas. According to *Jones et al.* [1998], the effect of mutual impedance will become negligible when the spacing between two dipoles is greater $2\lambda$ (two wavelengths).

Unfortunately, antennas that are further than $0.5\lambda$ apart introduce an ambiguity since an unknown number of multiples of $\pi$ are introduced [*Jones et al.*, 1998]. These ambiguities make it very difficult to mathematically solve the inverse problem of where the meteor scatter came from.

In this paper, we propose a new method for finding the direction of the meteor scatter, which takes into consideration all of the above errors and difficulties. This new method is a vast improvement over the traditional methods of interferometery, which can only determine the position of maximum likelihood of a meteor scatter. Our method can generate a map of the

likelihood of the meteor scatter across the whole sky. Furthermore, our method of interferometry easily accounts for phase errors due to mutual coupling and transmission line phase shifts. Unlike traditional interferometry, angle of arrival ambiguities and aliasing are not an issue with our method. For these reasons, this new method is a very useful tool for all meteor radar systems.

## 2. System Description

The Radar Remote Sensing Laboratory (RRSL) at the University of Washington is a passive radar system that uses the FM broadcasts in Seattle as its source signals [*Sahr and Lind*, 1997]. Since it operates in the FM band (88 MHz – 118 MHz), the wavelength (λ) of the signal is approximately 3 m. The antenna array consists of five Diamond D130-J discone antennas arranged in a cross, as shown in Figure 1. The array contains two orthogonal linear arrays of three antennas in which the central antenna has a spacing of about 3 m (1λ) to one antenna and a spacing of about 4.5 m (1.5λ) to the other. These two orthogonal linear arrays have a shared center antenna such that the whole array of five antennas looks like a cross. This configuration is a slight variation of the array presented in *Jones et al.* [1998]. The antenna numbering scheme shown in Figure 1 is used throughout the paper.

In order to conduct any type of interferometry, it is vital to know the exact positions of the antennas in the array. We have therefore made careful measurements of our array. In addition, we used an implementation of the Particle Swarm Optimization algorithm described in *Robinson and Rahmat-Samii* [2004] to determine the exact positions of our antennas based on our measurements. The ground plane is defined to be the xy-plane, with the center antenna directly above the origin. Table 1 shows the accepted coordinates of the feed point of each antenna in the array. The array described by these coordinates is used in all calculations throughout this paper, unless noted otherwise.

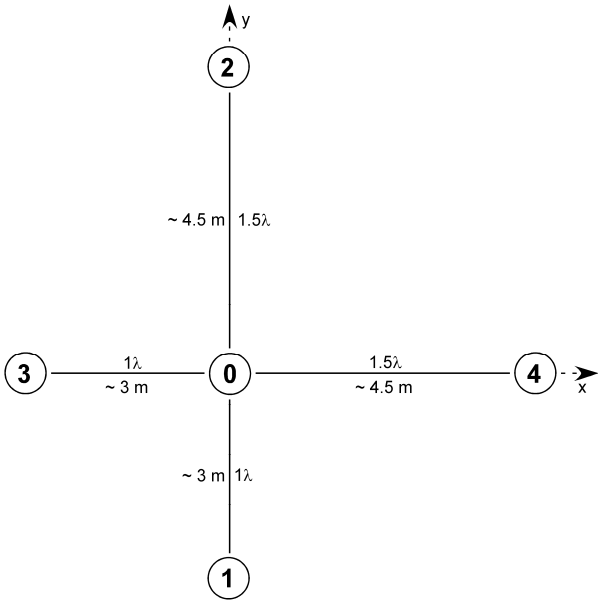


**Figure 1:** Discone antenna array; view from the z-axis. Distances indicated are all approximate.

**Table 1:** Cartesian coordinates of the feed point of each antenna in the discone array (in m)

| | x coordinate | y coordinate | z coordinate |
|---|---|---|---|
| Ant. 0 | 0.000 | 0.000 | 1.870 |
| Ant. 1 | 0.008 | -3.006 | 1.920 |
| Ant. 2 | -0.267 | 4.443 | 1.855 |
| Ant. 3 | -3.006 | -0.111 | 1.870 |
| Ant. 4 | 4.275 | 0.000 | 1.880 |

## 3. Phase Error in Transmission Lines

One source of phase errors is the phase shifts within the transmission lines that connect the antennas to the receiver. In order to counteract this effect, it is critical to know the exact electrical lengths of the cables that connect the antenna feeds to the receivers. If the length of cable is known, the voltages measured at the receivers can be adjusted to represent voltages at the antenna feed points.

### 3.1 Measurement of Cable Length

To measure the exact electrical lengths of the cables, we used an RF signal generator to produce a signal within a coaxial transmission line. Since the cable was open-circuited, this produced a standing wave that could be measured on an oscilloscope. By sweeping the signal generator in frequency across the FM band, we could measure which frequencies correspond to minimum amplitude standing waves on the oscilloscope (see Table 2). Using these measurements, the exact electrical length of each cable was determined using the method described below.

Since a standing wave has a period of π and any two consecutive minima of the standing wave differ by one waveform, then two consecutive minima must differ by π radians. If $L$ is defined to be the electrical length of transmission line, and $k$ to be the wavenumber of the standing wave, then it follows:

**Table 2:** Frequencies of minima of the standing wave in each cable (all ± 0.1 in MHz)

| Cable | $\nu_1$ | $\nu_2$ | $\nu_3$ | $\nu_4$ | $\nu_5$ | $\nu_6$ | $\nu_7$ | $\nu_8$ | $\nu_9$ | $\nu_{10}$ | $\nu_{11}$ |
|---|---|---|---|---|---|---|---|---|---|---|---|
| A | 77.8 | 85.9 | 94.1 | 102.3 | 110.5 | 118.7 | | | | | |
| B | 87.6 | 90.3 | 93.0 | 95.7 | 98.4 | 101.1 | 103.8 | 106.5 | 109.2 | 111.9 | 114.6 |
| C | 86.4 | 88.1 | 89.8 | 91.5 | 93.2 | 95.0 | 96.7 | 98.4 | 100.1 | 101.8 | 103.5 |

$$Lk_{n+1} - Lk_n = \pi$$

$$L\left(\frac{2\pi\nu_{n+1}}{c} - \frac{2\pi\nu_n}{c}\right) = \pi$$

because $k = \frac{2\pi}{\lambda} = \frac{2\pi\nu}{c}$

$$\frac{2\pi L}{c}\left(\nu_{n+1} - \nu_n\right) = \frac{2\pi L}{c}\Delta\nu = \pi \qquad (1)$$

By manipulating Equation (1), we can obtain cable length estimates using Equation (2):

$$L = \frac{c}{2\Delta\nu}, \qquad (2)$$

where $\Delta\nu$ is the difference in frequency between consecutive minima in the standing wave.

Additionally, because the cable was open circuited, there must be $N + 1/2$ wavelengths within the transmission line, where $N$ is a positive integer. If the data set contains $n$ values, then

$$k_n L = \frac{2\pi\nu_n}{c} L = \left(N_n + \frac{1}{2}\right)\pi \quad \forall n \qquad (3)$$

From Equation (2), the following equations for $N_n$ and $L$ can be obtained:

$$N_n = \frac{2\nu_n}{c} L - \frac{1}{2} \qquad (4)$$

$$L = \frac{c\left(N_n + 1/2\right)}{2\nu_n} \qquad (5)$$

Using the above equations, the following algorithm can be used to accurately determine the cable lengths.

1. Use $\Delta\nu$ to find an estimate for $L$, called $L_{est}$ using Equation (2). $L_{est}$ is the average of $n$-$1$ estimates for $L$ computed using Equation (2) for each $n$-1 frequency differences.
2. Use $L_{est}$ and $\nu_n$ to find $N_n$ for each $n$ using Equation (4). This gives $n$ values for $N_n$ which are very close to consecutive integers.
3. Use int($N_n$) and $\nu_n$ to find $L$ for each $n$ using Equation (5). This gives $n$ values for $L$ with only a very small deviation. These $n$ values are averaged to obtain a single value for $L$.

Table 3 shows the calculated cable lengths of the sample cables presented in Table 2. The average uncertainty of the cable length using this method is 0.10%. Even with a cable as long as 50 m, this method of estimating the cable length gives a length uncertainty of only 5 cm. At a 3 m wavelength, this corresponds to a 6° phase uncertainty, which is an acceptable level of error.

**Table 3:** Calculated electrical length of each cable.

| Cable | Length (in m) | Uncertainty (in m) |
|---|---|---|
| A | 18.314 | ± 0.019 |
| B | 55.600 | ± 0.055 |
| C | 87.614 | ± 0.092 |

## 3.2 Transmission Line Phase Shift Correction

The effect of the phase shifts inside of the transmission lines can easily be removed if the exact electrical length of each cable is known. The phase shift within a length $L$ of transmission line can be expressed as:

$$\phi = k\,L, \qquad (6)$$

where $k$ is the wavenumber of the signal traveling within the cable. Since $k$ is equivalent to $2\pi\nu$ / $c$, Equation (6) can be rewritten as:

$$\phi = \frac{2\pi}{c}\nu L, \qquad (7)$$

where ν is the frequency of the wave, and $c$ is the speed of light in free space. It should be noted that $L$ is the electrical length of the cable, and not the physical length.

The phase shift expressed by Equation (7) can be applied to the voltages measured by the receiver to remove the transmission line errors. Equation (8) represents the voltage on the antenna feed, $V_a$:

$$V_a = V_r \exp(-j\phi)$$
$$V_a = V_r \exp\left(\frac{-j2\pi\nu L}{c}\right) \quad (8)$$

where $V_r$ represents the voltage measured at the receiver. Using Equation (8), the effect of phase shifts in the transmission lines can be removed as long as the exact electrical length of the cable is known.

## 4. Phase Error due to Mutual Coupling

In addition to phase shifts within the transmission lines, phase errors can be introduced due to the mutual coupling between the antennas in an array. These errors can be very difficult to estimate and counteract, so many radar systems are built with large spacing between antennas to minimize the mutual coupling. *Jones et al.* [1998] suggests the minimum spacing between antennas should be no less than 2λ, since mutual coupling was found to be negligible at distances greater than 2λ. However, technical constraints forced our array to have antenna spacing as small as 1λ. To avoid significant errors from mutual coupling, we developed a method for determining the effect of mutual coupling.

Using the method of moments simulation called Numeric Electromagnetics Code (NEC) [*Burke and Poggio*], a computer model of the antenna array was created that could perform simulations to compute the effect of mutual coupling.

### 4.1 Building the NEC Model

Detailed measurements of the Diamond D-130J discone antenna were used to create a NEC computer model. Figure 2 shows the radiation pattern generated from the NEC model .

As a test of the model, NEC was used to generate a plot of the standing wave ratio (SWR) as a function of frequency. This plot is compared to the SWR plot created using a network analyzer connected the actual antenna (see Figure 3). From these plots, it is clear that the model is a very accurate representation of the actual antenna.

With confidence in the accuracy of the NEC model, the model of the entire array could be completed by duplicating the discones and placing each antenna at the correct location. The completed computer model can be used to aid in determining the likelihood of a meteor scatter event in each part of the sky.

### 4.2 Using the NEC Model

NEC simulations can be run to obtain the expected voltages measured at the feed point of each antenna for a meteor scatter event at a given location in the sky. A meteor scatter event can be approximated as a plane wave excitation of the antenna array [*Jones et al.*, 1998]. For this reason, each NEC simulation uses a circularly polarized plane wave excitation. The result of each simulation is a list of complex voltages that would be measured on each antenna feed, given the simulated plane wave excitation.

By varying the azimuth and elevation angle of the excitation, a large table of expected voltages for every point in the sky can be computed. Using 1° azimuth and elevation resolution, this table can be generated in only a few hours of simulation.

Because the NEC simulations are running a complete model of the array, all of the effects of mutual coupling are taken into consideration. The resulting table of voltages can be compared to live data from a real array to determine the likelihood that a meteor scatter event occurred at each position in the sky.

## 5. Determining Likelihood of Meteor Direction

The goal of meteor interferometry is to find the geophysical location of a meteor scatter event. This has traditionally been done by solving for the angle of arrival (AOA), which is computed as a function of the phase difference between two antennas, shown in Equation (9) as $\phi_{10}$ [*Jones et al.*, 1998]:

$$\phi_{10} = -2\pi \frac{d}{\lambda} \sin\xi \quad (9)$$

where, $d$ is the spacing between a two antennas, λ is the wavelength, and ξ is the angle of arrival (AOA).

Software can be used to calculate AOA solutions for each pair of antennas in the array. Then, all possible values for AOA are tested for each antenna pair to determine which solution matches for all pairs in the array. However, due to uncertainties, there is never a unique angle that satisfies Equation (9) for every pair

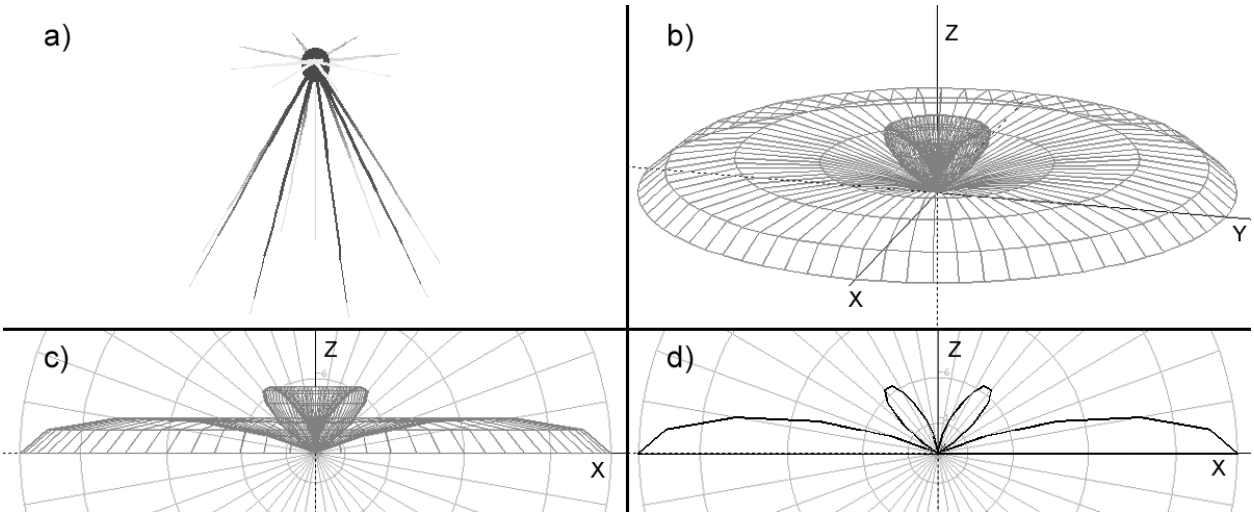


**Figure 2:** Radiation pattern at 97.3 MHz of a discone antenna 1.870 m above a perfectly conducting ground plane:
(a) Image of the NEC computer model of the antenna (showing currents flowing on the antenna's elements).
(b) Radiation pattern of the antenna.
(c) Radiation pattern viewed from xz-plane (same for any plane through z-axis due to rotational symmetry).
(d) Slice of radiation pattern at xz-plane (same for any plane through the z-axis due to rotational symmetry).

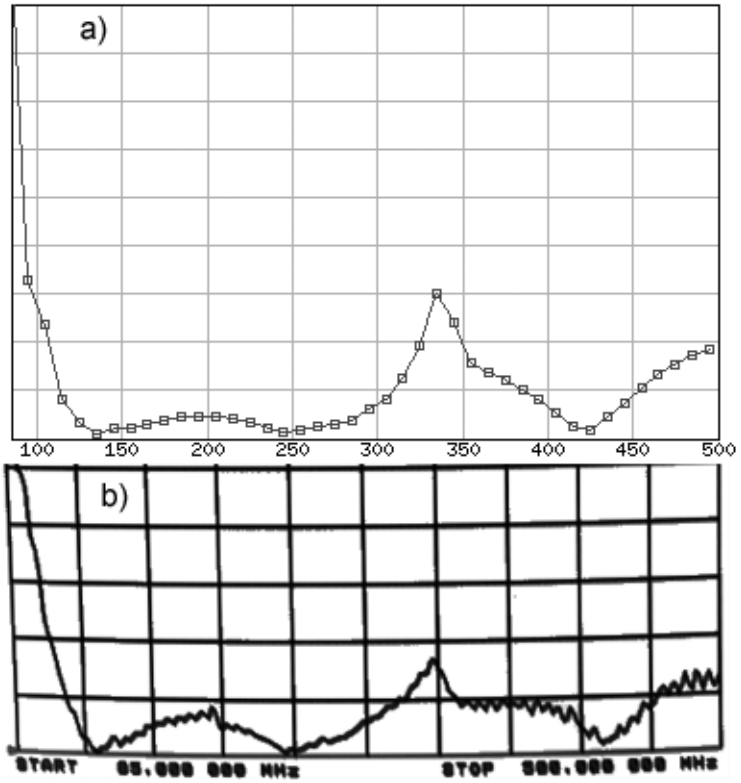


**Figure 3:** SWR plot comparison of NEC model and actual antenna. Frequency sweep from 85 to 500 MHz:
(a) SWR plot produced using NEC simulation
(b) SWR plot measured on an actual discone using a network analyzer

of antennas in an array. As a result, a value for AOA is traditionally accepted if it is within some error tolerance. Using a two dimensional array like one shown in Figure 1, it would then be possible to find azimuth and elevation angles describing the direction in the sky that a meteor event occurred [*Peña et al.*, 2005]. The traditional method of interferometery described above is referred to as solving the inverse problem.

This inverse problem approach works fairly well for systems with a high signal to noise ratio (SNR). However, for a system with a lower SNR, there may be more than one AOA value within the allowed error tolerances. Since the method of solving the inverse problem can only determine the location of greatest likelihood for an event, it is not acceptable to have multiple values for AOA that are within the tolerances. Solving the inverse problem also makes it difficult to account for phase errors due to coupling, which can be very difficult to quantify. In addition, it is often useful to know the likelihood of a meteor scatter across all parts of the sky, instead of only knowing the direction of greatest probability.

Our method solves the forward problem, by directly computing the likelihood of a meteor scatter event at every point in the sky. The general procedure for solving the forward problem is outlined below. Intermediate steps are explained in detail in the remainder of this section.

1. Create a computer model for the antenna array using NEC (see Section 4.1).
2. Compute expected voltages at the feed point of each antenna in the array by running NEC simulations using a plane wave excitation from each point in the sky (see Section 4.2).
3. Add the appropriate phase shift to all voltages calculated by the NEC model to accurately represent the phase shifts in the transmission lines (see Section 3.2).
4. Compute a list of antenna cross-correlations from the list of voltages obtained by the model (see Section 5.1).
5. Using real cross-correlation data from the actual array, compare the real data to the cross-correlations produced by the model (see Section 5.2).
6. Use a condensing function to obtain a single value for the likelihood of an event at each point in the sky (see Section 5.3).

## 5.1 Computing Cross-Correlations

All data produced by an interferometer is due to the cross-correlations between two antennas [*Sahr*, 1996]. Since the data sets produced by most interferometers are in terms of cross-correlations, it is easiest to compare the NEC model to real data if the model also produces cross-correlations.

The cross-correlation between antenna $m$ and antenna $n$ is defined in Equation (10):

$$R_{mn} = \left\langle V_m V_n^* \right\rangle \quad , \tag{10}$$

where $V_m$ is the complex voltage on antenna $m$, and $V^*_n$ is the complex conjugate of the voltage on antenna $n$. The $\langle \cdot \rangle$ notation represents an ensemble average in the time domain. An $n \times n$ matrix, $\mathbf{R}$, containing the correlations between all $n$ antennas can be created. The diagonal (when $m = n$) of $\mathbf{R}$ represents the self-correlation, or power on the $n$-th antenna, which is a real number. The elements below the diagonal are simply the complex conjugates of the corresponding elements above the diagonal ($\mathbf{R}_{mn} = [\mathbf{R}_{nm}]^*$). As a result of this symmetry, $\mathbf{R}$ contains only $n(n\text{-}1)/2$ independent cross-correlations, corresponding to the elements above the diagonal. Equation (10) is used to calculate the correlation matrix for each point in the sky using the table of complex voltages produced from the NEC simulations.

## 5.2 Comparing the Model to Real Data

Normalization of the cross-correlations is required in order to compare a real data set to the model. The normalized cross correlations, $r_{mn}$ are defined as:

$$r_{mn} = \frac{R_{mn}}{\sqrt{R_{mm} R_{nn}}} = \frac{R_{mn}}{\sqrt{P_m P_n}} \quad , \tag{11}$$

where $R_{mn}$ is the un-normalized correlation between antenna $m$ and antenna $n$. Since elements on the diagonal of $\mathbf{R}$ represent powers, $R_{mm}$ is written as $P_m$.

Once the correlation matrices of both the data and the model have been normalized using Equation (11), they can then be compared using a likelihood function. A likelihood function takes a difference between two cross-correlations and returns a value of likelihood between 0 and 1, where a value of 1 corresponds to the situation in which both cross-correlations are the same. There are several different likelihood functions that may be appropriate. Here, the uncorrelated Gaussian described by *Tarantola* [1987] is used:

$$L = \exp\left( -\left[ \frac{|\Delta r|}{\sigma} \right]^2 \right) \quad , \tag{12}$$

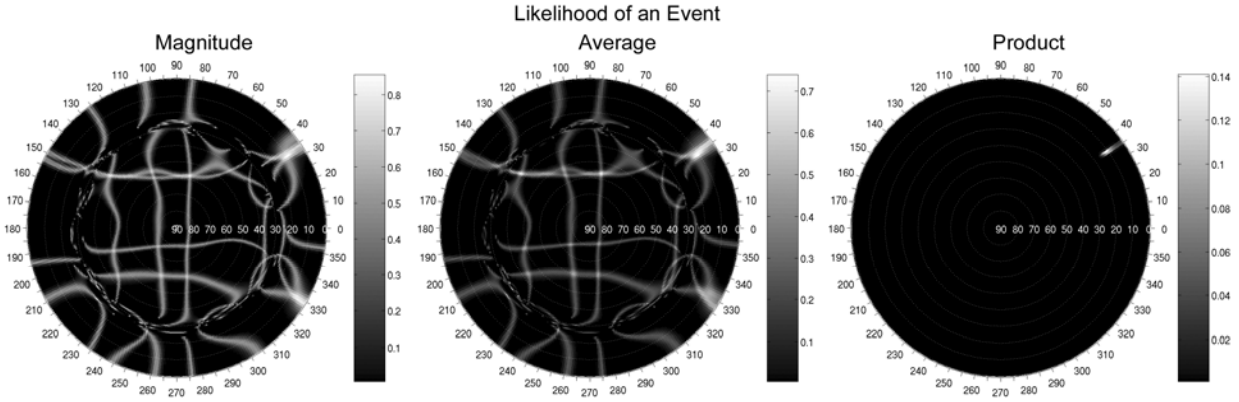


**Figure 4:** Likelihood plots comparing the three condensing functions when applied to the Gaussian likelihood function, where fake data plus random errors for a meteor located at 35° in azimuth and 10° in elevation was compared to the NEC model. The phase uncertainty was assumed to be 10°.

where $L$ is the value of likelihood, $|\Delta r|$ is the magnitude of the difference in the data and model cross-correlations, and $\sigma$ is the uncertainty in the cross-correlation data.

Calculating cross-correlation uncertainty ($\sigma$) is considerably difficult. Equation (13) shows a very basic approximation that should gives the correct order of magnitude:

$$\sigma_{mn} = \sqrt{\frac{P_m P_n}{N_{ind}}} \quad (13)$$

where $N_{\text{ind}}$ is the number of independent measurements taken in a time average of correlations. Like the cross-correlations, the uncertainties need to be normalized, yielding:

$$\sigma_{mn} = \frac{1}{\sqrt{N_{ind}}} \quad (14)$$

It should be noted that likelihood is not the same as probability, and thus these are not probability density maps of a meteor location. Nevertheless, likelihood is representative of probability and is therefore a useful measure.

## 5.3 Condensing Functions

After using a likelihood function, the result is a list of $n(n\text{-}1)/2$ independent likelihood values, where $n$ is the number of antennas in the array. The purpose of a condensing function is to obtain a single value to represent the likelihood of a meteor at the given position, instead of $n(n\text{-}1)/2$ different values. There are many functions that can be used for this purpose. We propose three such condensing functions: the magnitude, average, and product condensing functions.

The magnitude condensing function treats the list of likelihood values as a vector of length $\ell$, and returns the normalized magnitude of the vector. Equation (15) represents the magnitude condensing function, where $L_m$ is the output of the condensing function, and $l_i$ is the $i$-th element in the list of likelihoods:

$$L_m = \sqrt{\frac{\sum_{i=1}^{\ell} l_i^2}{\ell}} \quad (15)$$

The average condensing function returns the arithmetic mean of the list of likelihoods. The motivation is to produce a function that gives lower values when only one individual likelihood value is high. In other words, this function is more sensitive to multiple occurrences. Using the same variable definitions used in the preceding equation, Equation (16) represents the average condensing function:

$$L_a = \frac{\sum_{i=1}^{\ell} l_i}{\ell} \quad (16)$$

The product condensing function returns the product of each of the individual likelihoods in the list. This function is much more sensitive to multiple occurrences than either of the preceding ones. Therefore, it is ideal for finding the region of greatest likelihood. Using the same variable definitions as the preceding

equations, Equation (17) represents the product condensing function:

$$L_p = \prod_{i=1}^{\ell} l_i \qquad (17)$$

.

Figure 4 shows a comparison of the three condensing functions when applied to a set of test data. These plots show the likelihood of an event across the whole sky. The radial position in the plot represents the elevation angle, such that the center is the zenith and the edge is the horizon. The angular position around the circle represents the azimuth angle.

Each of the plots in Figure 4 represents a slightly different view of the situation. The magnitude condensing function shows the positions of all matches seen by the individual antennas, but shows multiple occurrences (positions where multiple antennas saw a good match) as a higher intensity. As expected, the average condensing model still shows all matches, but intensifies the multiple occurrences. As a result, the average condensing function is probably the most useful plot for mapping the likelihood across the whole sky. The product condensing function only shows the region representing the position of greatest likelihood.

## 6. Results

To obtain a likelihood plot based on real data from the five antenna array described in Section 2, correlation data was obtained at a frequency of 94.9 MHz. This is transmitting frequency of the local radio station KUOW, which was transmitting from an azimuth of 244° and an elevation slightly above the horizon. Figure 5 shows the likelihood plot created from this data. As expected, there is a strong likelihood that the signal came from an azimuth of 243° and an elevation of 20°. Although this position is not the direction of maximum likelihood it is very promising that this method of interferometry is able to identify the correct position of the transmitter.

We have only begun our investigation into this method of interferometry, and as a result many other effects still need to be considered. One major effect to consider in the future is multi-path. It is known that radio waves are actually arriving from many different directions, and not just from one position in the sky. Therefore, more analysis is necessary in order to make this interferometer a reliable technique for meteor radar interferometry. As an additional improvement, we suggest the application of closure phase and closure amplitude in both temporal and spatial domains [*Sahr*, 1996].

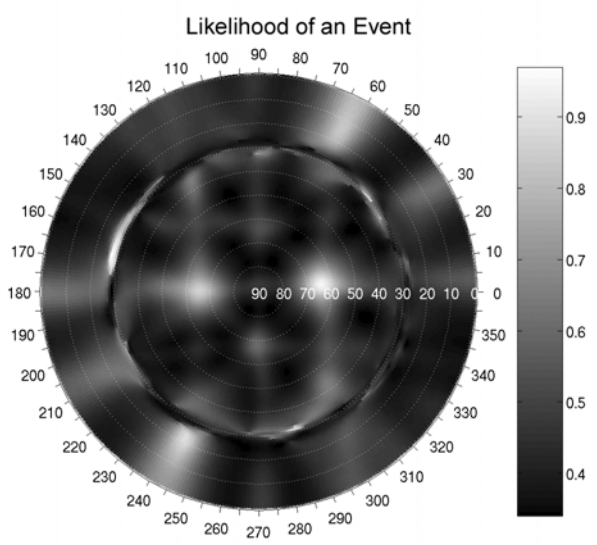


**Figure 5:** Likelihood plot created from 1 sample of correlation data taken on 94.9 MHz and compared to the NEC model of the array. The Gaussian likelihood function and the average condensing function were used to produce this plot.

## 7. Summary

We conducted an investigation into the phase errors associated with phase shifts in transmission lines as well as errors from mutual coupling between antennas in an array. This investigation resulted in the formation of a new method of meteor radar interferometry.

The new method of interferometry is a vast improvement over the traditional interferometry, because it gives not only the position of maximum likelihood of the meteor scatter, but also a map of the likelihood of meteor location across the whole sky. In addition, this new method of interferometry accounts for phase errors due to mutual coupling and transmission line phase shifts. Unlike traditional interferometry, angle of arrival ambiguities and aliasing are not an issue with our method. For these reasons, this new method is a very useful tool for all meteor radar systems.

**Acknowledgement.** The authors are grateful for support from National Science Foundation Division of Atmospheric Sciences (award ATM-0310233).

## References

Burke, G. J., and A. J. Poggio, Numerical Electromagnetic Code (NEC) - Method of Moments, NOSC Technical Document 116, Naval Ocean Systems Center, Jan. 1980.

Holdsworth, D. A., M. Tsutsumi, I. M. Reid, T. Nakamura, and T. Tsuda (2004), Interferometric meteor radar phase calibration using meteor echoes, *Radio Sci.*, *39*, RS5012, doi:10.1029/2003RS003026.

Jones, J., A. R. Webster, and W. K. Hocking (1998), An improved interferometer design for use with meteor radars, *Radio Sci.*, *33*(1), 55-65.

Meyer, M. G., and J. D. Sahr (2004), Passive coherent scatter radar interferometer implementation, observations, and analysis, *Radio Sci.*, *39*, RS3008, doi:10.1029/2003RS002985.

Peña, d. l., Santiago, S. K. Avery, J. P. Avery, E. Lau, and D. Janches (2005), Wind measurements of MLT region using the Platteville, CO MEDAC 50 MHz meteor radar, *J. Atmos. Terr. Phys.*, *67*, 1211 -1215.

Robinson, J., and Y. Rahmat-Samii (2004), Particle Swarm Optimization in Electromagnetics, *IEEE Trans. Ant. Prop.*, *52*(2), 397-407.

Sahr, J. D. (1996), Application of closure phase and self-calibration to radar interferometric imaging of atmospheric and ionospheric irregularities, *J. Atmos. Terr. Phys.*, *58*(8/9), 959-964.

Sahr, J. D., and F. D. Lind (1997), The Manastash Ridge radar: A passive bistatic radar for upper atmospheric radio science, *Radio Sci.*, *32*(6), 2345 –2358.